



Structural, optical and electrochemical properties of banana, mango leaves and potato extracts reduced graphene oxide

SAYANTAN SINHA, KANHU CHARAN ANDIA, NAOREM ARUNA DEVI
and BIBHU PRASAD SWAIN* 

Department of Physics, National Institute of Technology Manipur, Imphal West, Manipur 795004, India

*Author for correspondence (bibhuprasad.swain@gmail.com; bpswain@nitmanipur.ac.in)

MS received 6 May 2022; accepted 25 July 2022

Abstract. Green synthesis of reduced graphene oxide (rGO) was done using three different plant extracts, such as banana, mango leaves and potato, as the reducing agent. The field-emission scanning electron spectroscopy revealed the formation of thin layers in the morphology of rGO reduced with the green extracts. The X-ray diffraction patterns reveal that the peak for GO (001) appeared at $2\theta = 11.01^\circ$ and in rGO broad peak appeared for the (002) plane at $\sim 21^\circ$ – 26° . The Fourier transform infrared spectroscopy graphs showed the peaks for C=C at $\sim 1571\text{ cm}^{-1}$, which confirmed the formation of the graphene backbone structure. Raman analysis showed the characteristic G band for the sp^2 carbon structure of rGO. The cyclic voltammetry study revealed that the rGO-b exhibits the most significant value of specific capacitance of 176 F g^{-1} at a 5 mV s^{-1} scan rate.

Keywords. rGO; green synthesis; eco-friendly reduction; supercapacitor; graphene.

1. Introduction

Graphene is the one-layer carbon structure with an sp^2 hybridized honeycomb lattice structure. Because of its exceptional mechanical, optical, thermal and electrical properties, graphene has been an attractive material of choice in various fields such as supercapacitor, sensor, solar cell, field-effect transistor, etc. [1–4]. The various approaches to synthesizing graphene are typically categorized into top-down and bottom-up. The bottom-up approach, which includes pyrolysis, epitaxial growth technique, chemical vapor deposition, etc., is slower and unsuitable for industry-scale production. On the other hand, a top-down approach involving mechanical and chemical exfoliation is a scalable technique and feasible for prototyping and large-scale production. Among the various approaches to synthesizing graphene, the chemical reduction process of graphene oxide (GO) has achieved the utmost popularity because of its scalability, simplicity and inexpensiveness. Hydrazine hydrate and sodium borohydride are the conventional chemical reducing agents [5,6]. Nevertheless, these are toxic and potentially dangerous for our environment. Also, after the reduction process, the final product may contain some traces of those toxic chemicals, which makes it inapplicable in most biological fields.

Many researchers have reported green reduction processes for reduced graphene oxide (rGO) synthesis to

alleviate these problems. Bhattacharya *et al.* [7] described a green synthesis process for rGO using aloe vera extract as the reducing agent and used the rGO for dye removal application. Bo *et al.* [4] utilized caffeic acid to synthesize rGO and used the rGO for electrochemical storage and sensing application. Moosa and Jaafar [8] synthesized rGO with the help of tea leaves extracts and explored its application in lead ion removal from aqueous solution. Zhang *et al.* [9] reported GO reduction using L-ascorbic acid. Suresh *et al.* [10] synthesized rGO using cloves extract as a reducing agent and investigated the antioxidant and dye degradation properties of the rGO. Kuila *et al.* [11] employed carrot root as a reducing agent to synthesize rGO.

Although various green reducing agents in place of harmful chemical reductants have been investigated by several research groups for synthesizing rGO, many of them are coming from expensive sources such as cloves, carrots, tea leaves, etc. Since, a green reducing process is to be adoptable in the industry, it should be economically viable too, the necessity for the search of the green reducing agents having abundance in a particular geographical location is still very important. Also, many times the characteristics of the rGO such as morphology, electrical, optical, mechanical properties, etc. differ for using different reducing agents. These might lead to affect the performance of the yield in a specific application. Therefore, it is also necessary to carry out a comparative performance study of the rGO prepared

with different reducing agents in a particular field of application.

The above motivations lead to our present work, where we used three different green reducing agents, banana peel, mango leaves and potato extracts as eco-friendly substituents for the toxic chemical reductants. Among which banana peel is often discarded and thrown away without any use and mango leaves and potato have their abundance in the major parts of India. This study also focuses on the investigation of various characteristics of the green reduced rGO samples such as morphology, elemental properties, structural properties, chemical bonding, and optical properties. This work also reveals a comparative study of the rGO with different green reductants for the supercapacitive application via electrochemical analyses.

2. Experimental

2.1 Materials used

Graphite powder, sodium nitrate (NaNO_3) (Sigma-Aldrich), sulphuric acid (H_2SO_4 , 98%), hydrogen peroxide (H_2O_2 , 30% v/v) (Merck), potassium permanganate powder (KMnO_4) (Merck), hydrochloric acid (HCl , 35%) (Sigma-Aldrich), ripped banana and potato (collected fresh from the local market), and green mango leaves.

2.2 GO synthesis

GO synthesis was done using a modified Hummer's method [5,12]. A quantity of 3 g of fine graphite powder was added with 1.5 g of NaNO_3 . Then 66 ml of concentrated H_2SO_4 was poured into it and stirred for up to 30 min, keeping in an ice bath. After that, 9 g, KMnO_4 was slowly added, strictly maintaining the temperature below 20 °C. Then 150 ml of de-ionized (DI) water was slowly added and the temperature was raised to 98 °C. Then it was allowed to be stirred until 1 h. After that, 250 ml of DI water was added and then 15 ml of H_2O_2 was added to kill the reaction. On the next day, the orange precipitate was washed using 10% HCl solution to remove the residual metal ions and then washed multiple times using DI water until the pH value reached close to neutral. Then the filtrate was left to dry in a hot-air oven for 24 h at 40 °C. After drying, it was ground using mortar-pestle and GO powder was obtained.

2.3 Preparation of banana peel extract

Ripped bananas were washed with warm water first. Then the peels were collected and cut into small pieces. The peels were mixed with DI water and grinded in a kitchen grinder,

filtered using filter paper. The filtrate was collected as the banana extract.

2.4 Preparation of mango leaves extract

Freshly collected mango leaves were washed with warm DI water to remove the dirt from the leaves. Then the leaves were dried keeping in a hot-air oven at 60 °C for 12 h so that they could be crushed easily in the next step. The dried leaves were then grinded to powder and mixed with DI water in a 1:10 ratio. Then it was stirred for 2 h at 50 °C. This was done to extract the several polyphenols present in the mango leaves, which have reducing properties [13]. After that, the solution was filtered and the filtrate was the desired mango leave extract.

2.5 Preparation of potato extract

The fresh potato was thoroughly washed with DI water and peeled off. After that, the potato was sliced into thin pieces and washed with warm DI water to remove most of the starches. The sliced potato was then mixed with 100 ml DI water and grinded. The potato extract was obtained as the filtrate after filtering that paste.

2.6 Synthesis of rGO using banana extract

A quantity of 200 mg of GO powder was dispersed into 500 ml of DI water by stirring for 2 h at room temperature. Then 40 ml of banana extract was added and stirred for 24 h at 90 °C under reflux conditions. The dispersion colour changed from orange-brown to black during the stirring process, indicating that the reduction occurred. Then the black rGO was filtered, washed with DI water, and dried in the oven at 40 °C for 12 h.

2.7 Synthesis of rGO using mango leave extract

The 200 mg GO was dispersed into 500 ml DI water as previously and 40 ml of mango leave extract was added. The rest of the process was the same as the banana extract reduction.

2.8 Synthesis of rGO using potato extract

After dispersing 200 mg of GO into 500 ml of DI water and 40 ml of potato, the extract was added, and a similar method was followed as described in the cases of banana and mango leaves extract.

3. Characterizations

The material surface morphology was analysed using a field-emission scanning electron spectroscopy (FESEM), model no (JEOL JSM-6700F). The structural analysis was performed with the help of powder X-ray diffraction (XRD; Bruker D8 Advance) at a scan rate of 1° s^{-1} . The elemental analysis was done using energy-dispersive X-ray spectroscopy. A functional group study was carried out using Fourier transform infrared (FTIR) spectroscopy (PerkinElmer Spectrum Two) with the IR spectrum wavenumber ranging from 400 to 4000 cm^{-1} . The Raman analysis (Horiba Jobin Vyon, Model LabRam HR) was employed to study the chemical bonding structure (excitation wavelength = 514 nm). The optical properties were studied using photoluminescence (PL) and UV-visible spectroscopy (UV-vis). The electrochemical performance was measured using cyclic voltammetry (CV), galvanostatic charge-discharge (GCD) and electrochemical impedance spectroscopy (EIS) techniques. The CV was performed with varying scan rates ranging from 5 to 100 mV s^{-1} . The GCD analysis was carried out with different

current densities in the range of $2\text{--}5 \text{ A g}^{-1}$. The frequency response data in the EIS study was recorded with varying the frequency from 100 kHz to 0.1 Hz. The ac amplitude was kept fixed at 10 mV with a dc offset of 0 V.

4. Results and discussion

4.1 FESEM analysis

Figure 1 shows the FESEM micrographs of GO and rGO reduced using banana extract (rGO-b), mango extract (rGO-m) and potato extract (rGO-p). The morphology of GO shows a clustered structure, while rGO-b, rGO-m and rGO-p show thin-layered structures in their morphology. Among the rGO-b, rGO-m and rGO-p, rGO-b has shown thinner flakes and more significant gaps between them, which indicates a better reduction of GO. The surface roughness was estimated using Gwyddion software, which statistically computes it from the second central moment of the image data values. The surface roughness was obtained as 137.3, 211.6, 156.0 and 156.8 nm for GO, rGO-b, rGO-m and rGO-p, respectively. Surface roughness is a significant parameter for electrochemical

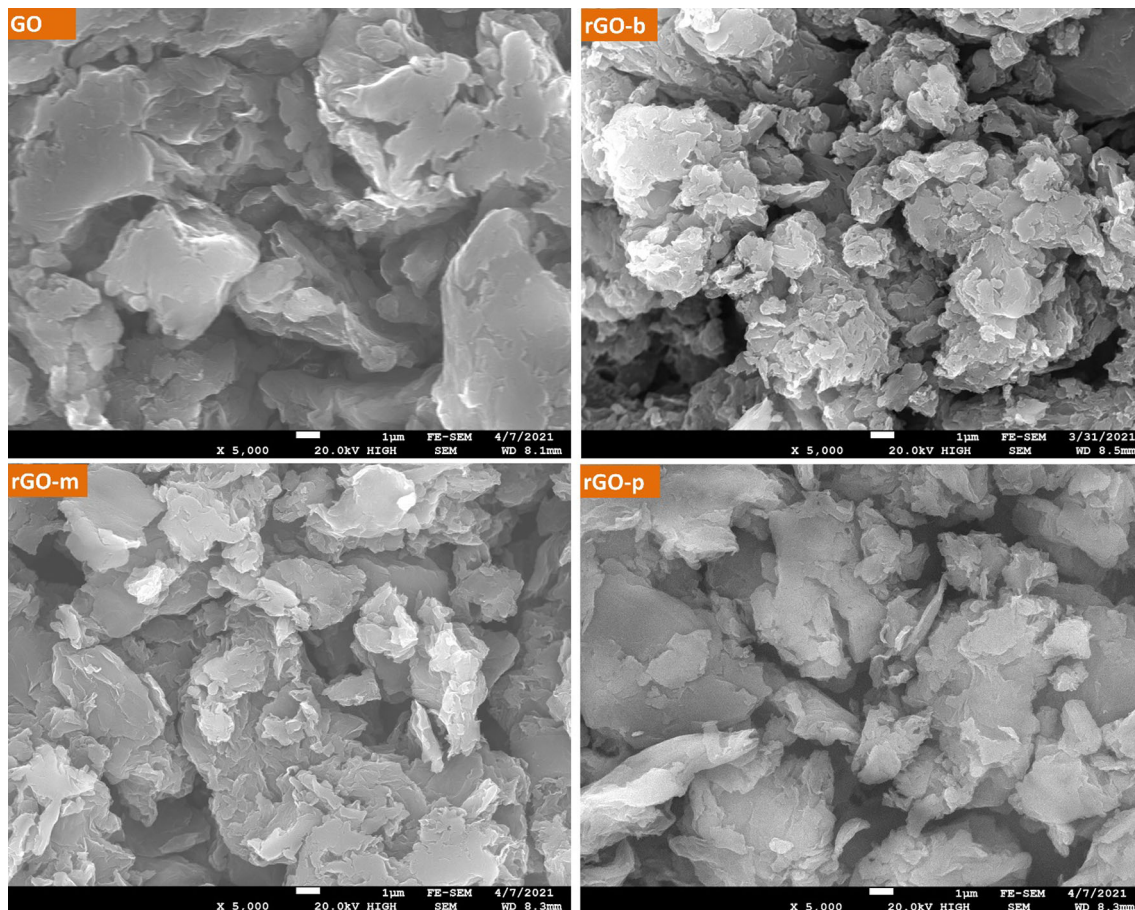


Figure 1. FESEM images of GO, rGO-b, rGO-m and rGO-p.

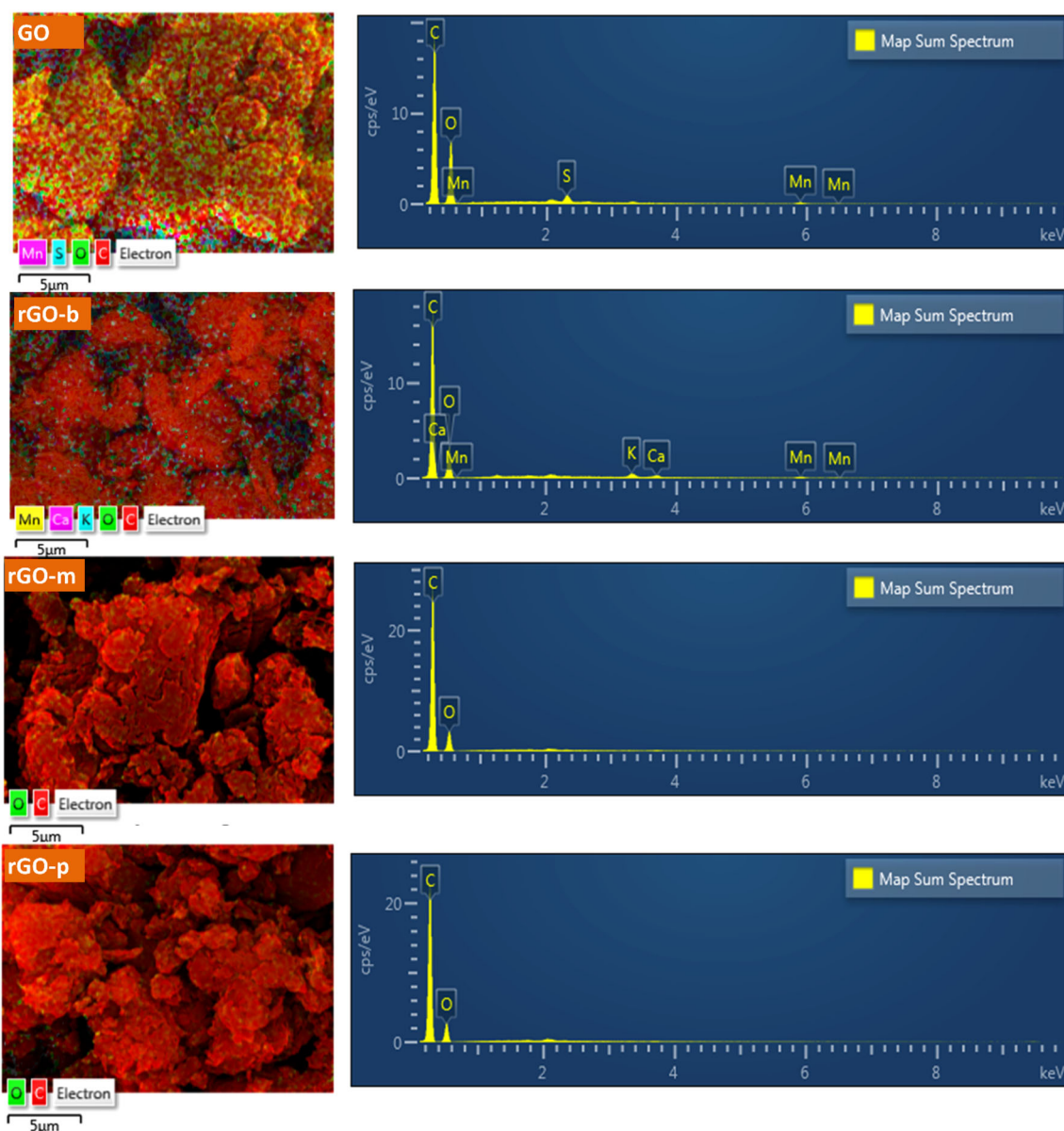


Figure 2. Colour-mapped energy-dispersive X-ray images of GO, rGO-b and rGO-m.

application because higher surface roughness means a higher active surface area for electrochemical reactions.

4.2 Energy-dispersive X-ray analysis

Figure 2 shows the energy-dispersive X-ray colour-mapped images for GO, rGO-b, rGO-m and rGO-p. GO shows that a large amount of oxygen is distributed along with carbon over the surface. The estimated at% of C, O, S and Mn were 66.85, 32.6, 0.37 and 0.18. The minute trace of S and Mn in GO might be coming from the H_2SO_4 and KMnO_4 , respectively, used during the synthesis process. In rGO-b, C, O, K, Ca and Mn were found with at% of 78.6, 20.7, 0.3, 0.18 and 0.22, respectively. The at% of C and O in

rGO-m were 78.95 and 21.05, respectively. In rGO-p, the at% of C and O were 79.02 and 20.98, respectively. The C/O ratio in GO, rGO-b, rGO-m and rGO-p were 2.05, 3.80, 3.75 and 3.77, respectively, which showed a slightly better reduction of rGO-b compared to that of rGO-m and rGO-p. The C/O ratios also show that the amount of oxygen is reduced in rGO-b, rGO-m and rGO-p in comparison to GO, which confirms the reduction of GO. The banana peel extract may contribute to the small traces of Ca and K in rGO-b, which is a rich source of dopamine, L-dopa and catecholamines [14], which have an excellent reducing effect. Banana peel extract contains many estragole, ethyl ester, epicatechin, gallic acid and hexadecanoic acid [15]. Those phytoconstituents in high amounts of banana peel may be a probable reason for performing as

a reducing agent slightly better than potato and mango leaves extract.

4.3 XRD analysis

Figure 3 illustrates the XRD patterns of GO, rGO-b, rGO-m and rGO-p. A sharp peak was observed corresponding to the GO(001) plane at $2\theta = 11.01^\circ$. The crystallite size was calculated as 1.17 nm, and the d-spacing was 0.804 nm. In the rGO-b, the sharp GO peak got absent and a new broad peak appeared at $2\theta=22.89^\circ$, corresponding to the rGO(002) plane. The crystallite size and d-spacing for the rGO(002) plane were 1.66 and 0.39 nm. The decrease of d-spacing in rGO from 0.803 to 0.39 nm signifies the efficient reduction of the oxygen functional groups from GO [4]. rGO(002) was found at $2\theta = 25.53^\circ$ for rGO-m, from which the crystallite size and d-spacing were calculated as 1.32 and 0.35 nm, respectively. The rGO-p shows the rGO(002) plane at $2\theta = 21.34^\circ$. The crystallite size and d-spacing were obtained as 1.18 and 0.42 nm, respectively.

4.4 Analysis of FTIR spectroscopy

Figure 4 shows the FTIR plots for GO, rGO-b, rGO-m and rGO-p. In GO, a broad absorption peak appeared at 3607.8 cm^{-1} , which attributed to the stretching vibration of the -OH bond. A peak corresponding to C=O stretching, C=C and O-H deformation peaks were obtained at 1729.4, 1623.0 and 1368.0 cm^{-1} , respectively. The absorption peaks associated with C-O(epoxy) and C-O(alkoxy) were observed at 1218.7 and 1052.1 cm^{-1} , respectively [11,16]. After GO reduction, C=C peak intensity has increased significantly and the wavenumber corresponding to the C=C stretching is shifted to ~ 1571 from 1623.0 cm^{-1} . The presence of C=C indicates the existence of an sp^2 hybridized carbon network, which is the backbone structure of graphene layers. In rGO, the -OH stretching vibration (3607.8 cm^{-1}) peak became much smaller or even absent in some cases compared to GO, because most of the oxygenated functional groups were removed. The peak positions of C-O(epoxy) and C-O(alkoxy) were slightly shifted in rGO. However, they did not disappear because a few amounts of oxygen groups remained after the reduction process. The O-H deformation peak is prominent in GO but almost absent in rGO spectra. These observations indicate the formation of rGO by reducing GO.

4.5 Analysis of Raman spectroscopy

Figure 5 illustrates the Raman bands for rGO-b, rGO-m and rGO-p. The Raman peaks were empirically deconvoluted into four Gaussian peaks [17]. The D-band resembles the breathing mode of j-point phonons of A_{1g} symmetry

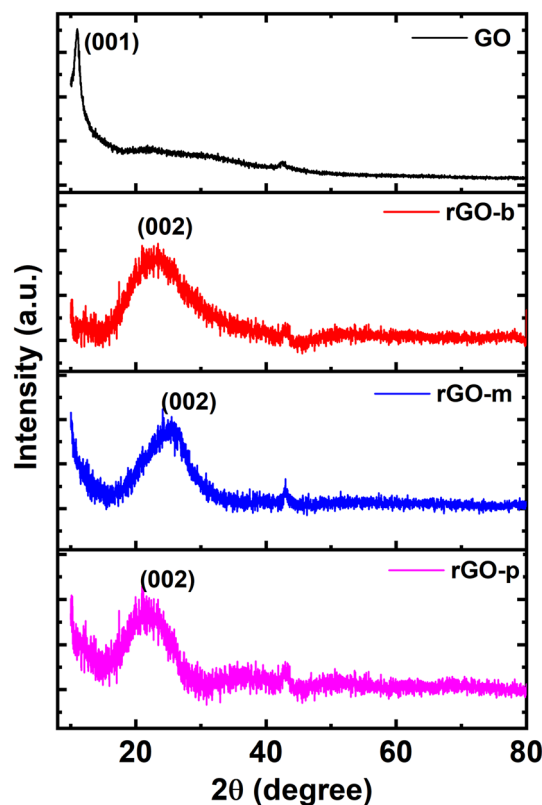


Figure 3. XRD patterns for GO, rGO-b, rGO-m and rGO-p.

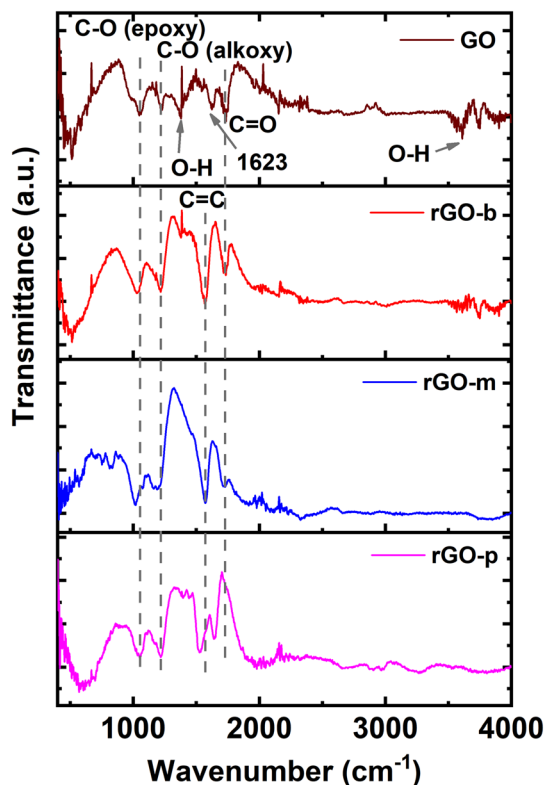


Figure 4. FTIR spectra for GO, rGO-b, rGO-m and rGO-p.

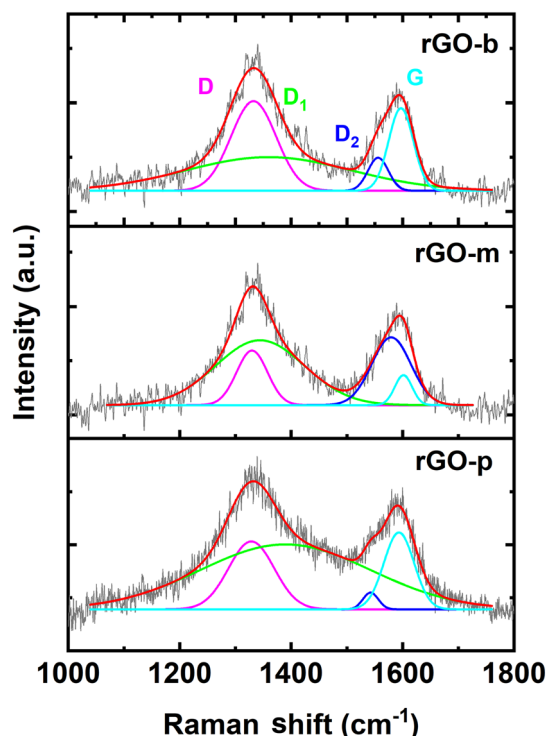


Figure 5. Raman spectra of rGO-b, rGO-m and rGO-p.

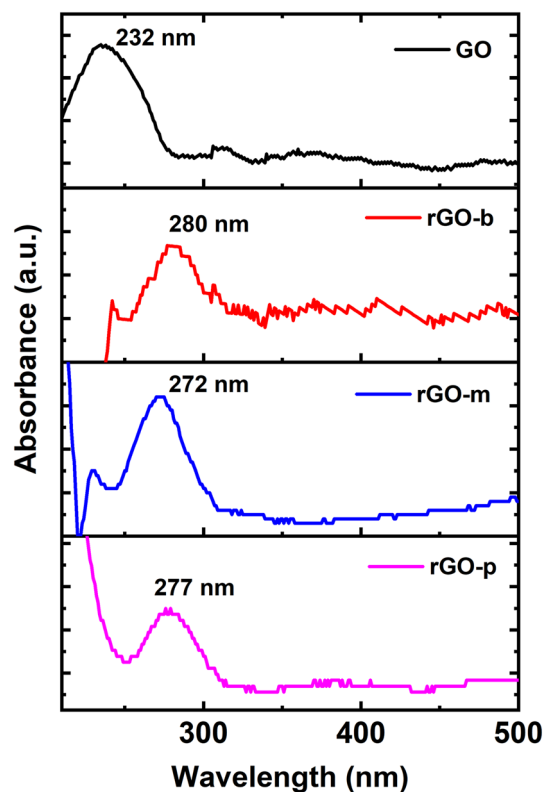


Figure 7. UV-vis spectra of GO, rGO-b, rGO-m and rGO-p.

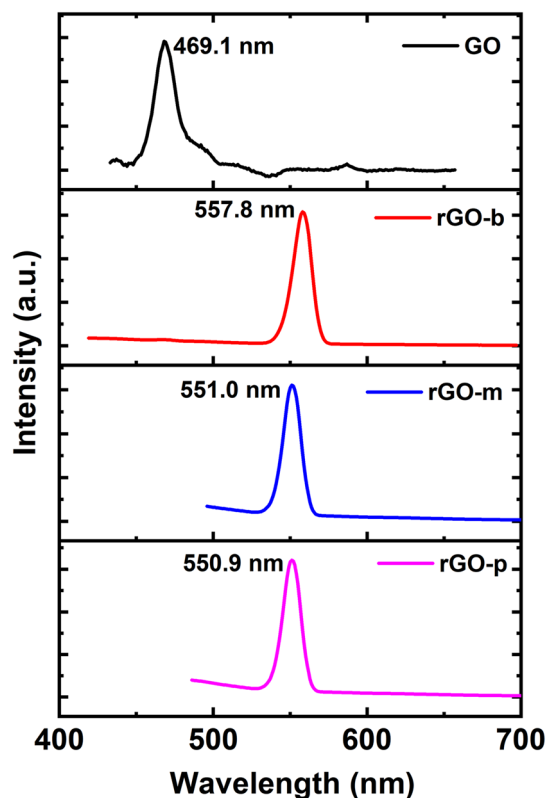


Figure 6. PL spectra of GO, rGO-b, rGO-m and rGO-p.

obtained at 1332.6, 1329.9 and 1328.7 cm^{-1} for rGO-b, rGO-m and rGO-p, respectively. The D_1 peak, which attributes to the sp^2 - sp^3 defects in the rGO structure, appeared at 1359.6, 1344.4 and 1389.9 cm^{-1} for rGO-b, rGO-m and rGO-p, respectively. The D_2 peak attributing to the functional group defects was observed at 1556.2, 1579.7 and 1542.7 cm^{-1} for rGO-b, rGO-m and rGO-p, respectively [18]. The G-band, which attributes to the first-order E_{2g} phonon scattering of the sp^2 carbon, appeared at 1597.1, 1601.5 and 1593.4 cm^{-1} for rGO-b, rGO-m and rGO-p, respectively [11,12,19]. The I_D/I_G ratio is a normalized value indicating the disorder in the sp^2 carbon structure and was obtained to be 2.22, 1.98 and 1.34 for rGO-b, rGO-m and rGO-p, respectively.

4.6 PL analysis

Figure 6 shows the PL spectra obtained for GO, rGO-b, rGO-m and rGO-p, which shows the PL peaks at 469.1, 557.8, 551.0 and 550.9 nm for GO, rGO-b, rGO-m and rGO-p, respectively. The PL peaks have been assigned to the π - π^* transition of electrons in the sp^2 carbon structure. Since attaching the oxygen functional groups to the graphene structure, some sp^2 bond structures are converted to the sp^3 structure. The PL peak in GO has been shifted towards the lower wavelength (higher photon energy) than

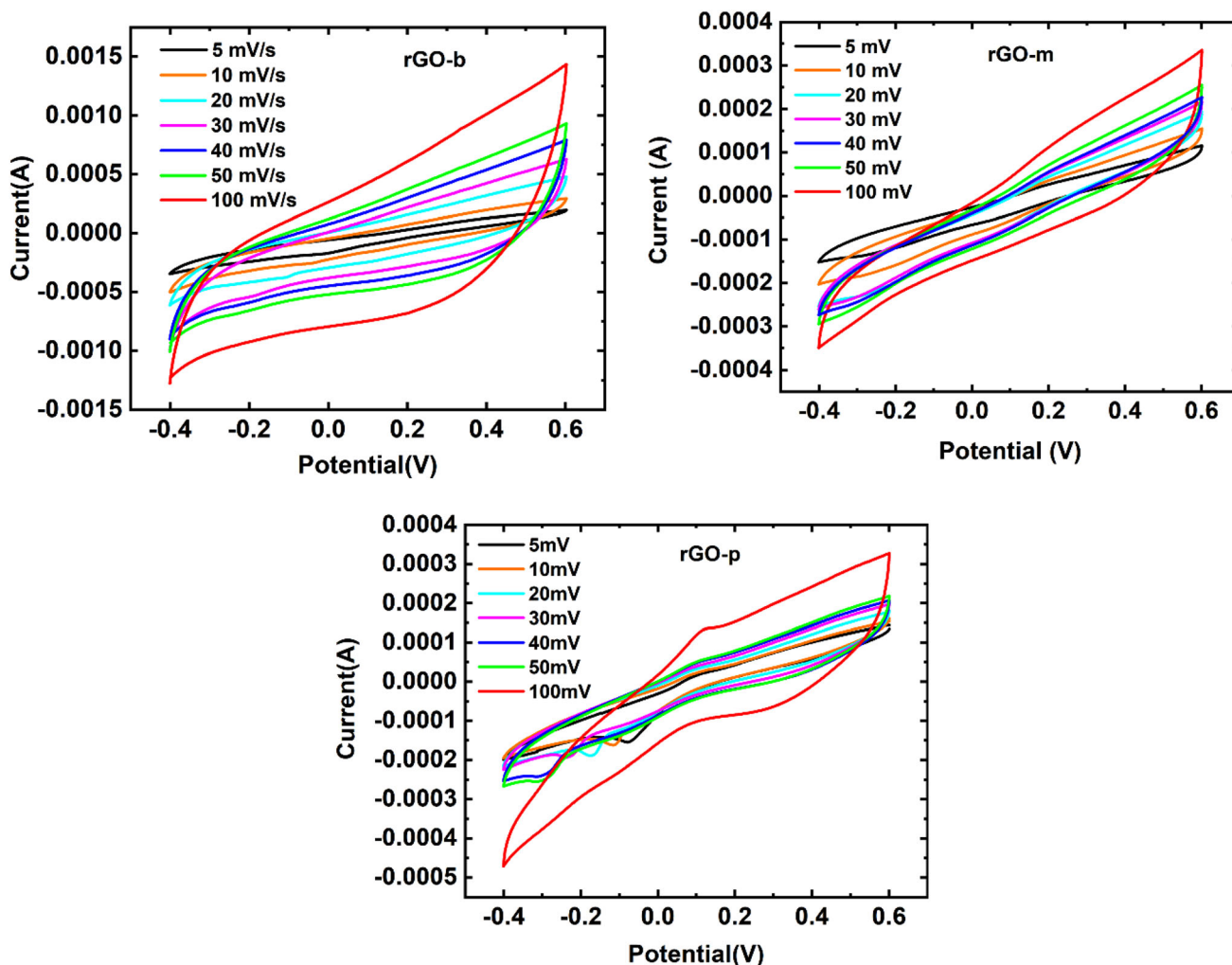


Figure 8. Cyclic voltammogram of rGO-b, rGO-m, and rGO-p at different scan rates.

Table 1. Specific capacitance was obtained from CV at different scan rates for rGO-b, rGO-m and rGO-p (values are in F g⁻¹).

Sample name	s.r. (mV s ⁻¹)						
	5	10	20	30	40	50	100
rGO-b	176	119	80	74	63	58	43
rGO-m	87	58	36	25	19	16	10
rGO-p	113	58	31	21	17	14	12

resembles $\Delta E = 1240/\lambda$. The average interval between the excitation and photon radiation is the decay lifetime or Δt . From the PL data it was observed that $\Delta E = 2.64$ eV for GO, 2.22 eV for rGO-b, 2.25 eV for rGO-m and 2.25 eV for rGO-p. The average decay lifetime $\Delta t = 0.124, 0.148, 0.146$ and 0.146 fs for GO, rGO-b, rGO-m and rGO-p, respectively. A slower recombination velocity in rGO-b than GO, rGO-m and rGO-p might be due to the higher surface state density and, consequently, more band-edge nonradiative recombination in rGO-b.

rGO [20]. From the uncertainty principle of Heisenberg for energy and time dispersion

$$\Delta E \Delta t \geq \frac{\hbar}{2}, \tag{1}$$

where ΔE and Δt are the energy and time uncertainty, respectively [21]. When an excited atom makes the downward transition through electronic states, energy is radiated as photons with a specific wavelength λ . That energy

4.7 UV-vis analysis

Figure 7 displays the UV-vis graphs for GO, rGO-b, rGO-m and rGO-p. The GO spectrum exhibits the peak of absorption at 232 nm, which corresponds to the $\pi-\pi^*$ electronic transition within the C=C bonds [7,22]. In the rGO-b, the absorption peak was observed at 280 nm. The absorption peaks were obtained at 272 and 277 nm for rGO-m and rGO-p, respectively, with the different reducing agents. The

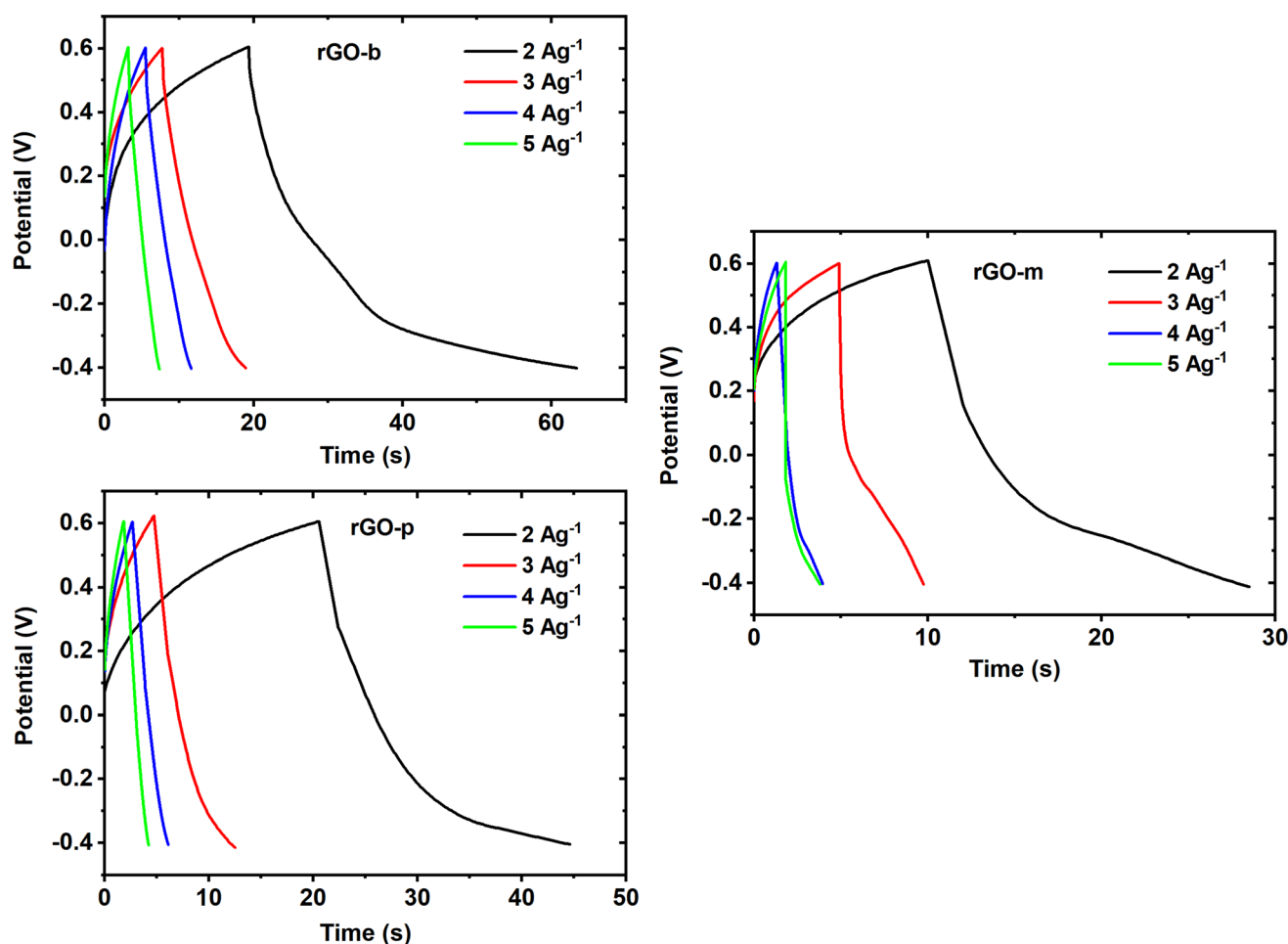


Figure 9. Galvanostatic charge–discharge curves for rGO-b, rGO-m and rGO-p at different current densities.

Table 2. Specific capacitance obtained from GCD for rGO-b, rGO-m and rGO-p at different current densities varying from 2 to 5 A g⁻¹ (SC values are in F g⁻¹).

Sample name	Current density (A g ⁻¹)			
	2	3	4	5
rGO-b	88.2	33.8	25.1	24.6
rGO-m	37.8	15.3	11.8	10.5
rGO-p	48.0	23.4	13.6	12.5

absorption peaks in rGO were red-shifted from 232 nm in GO to 272–280 nm, probably due to eliminating oxygenated functional groups and the formation of more sp² bonds [7]. From that observation, it is indicated that the rGO-b was reduced better than rGO-m and rGO-p.

4.8 Electrochemical analyses

Figure 8 shows the cyclic voltammogram for GO, rGO-b, rGO-m and rGO-p at different scan rate (s.r.) from

5 to 100 mV s⁻¹. The specific capacitance (SC) was calculated using equation (2).

$$SC = \frac{\text{Area under the CV curve}}{m \times \Delta V \times s.r.}, \quad (2)$$

where ΔV = potential window, and m = active material mass.

Table 1 shows the SC values for different materials at different s.r. rGO-b showed the maximum SC value of 176 F g⁻¹ at 5 mV s⁻¹ s.r., followed by rGO-p (113 F g⁻¹) and rGO-m (87 F g⁻¹).

Figure 9 depicts the GCD curves at different current densities ranging from 2 to 5 A g⁻¹ for rGO-b, rGO-m and rGO-p. The SC was calculated from the GCD analysis using equation (3).

$$SC = \frac{I \times t}{m \times \Delta V}, \quad (3)$$

where I = current passing through the working electrode, t = capacitor discharge time, ΔV = potential window, and m = active material mass.

Table 2 summarizes the SC values obtained at different current densities for different materials. From GCD

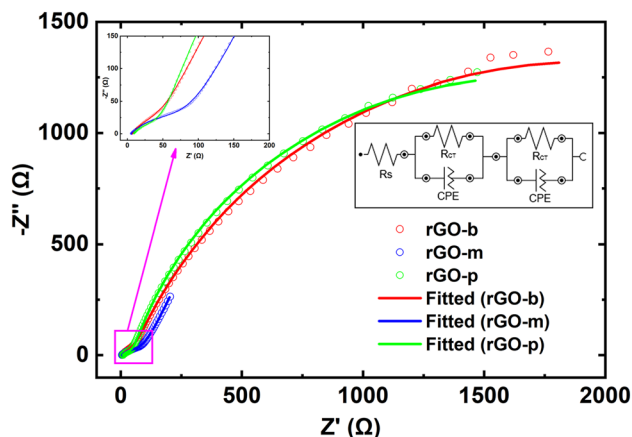


Figure 10. Nyquist plots for rGO-b, rGO-m and rGO-p.

analysis, rGO-b, rGO-m and rGO-p exhibited SC of 88.2, 37.8 and 48.0 F g⁻¹, respectively, at a current density of 2 A g⁻¹. Hence, the SC for different materials as obtained employing CV and GCD follow the same trend.

Figure 10 shows the Nyquist plots for rGO-b, rGO-m and rGO-p. In the inset, the semi-circular part at the high to mid frequency range has been zoomed in. The curves were fitted using Nova 2.0 software with the simulation data of the empirical equivalent circuit, as shown in the inset. Table 3 lists the electrochemical series resistance R_s , the charge transfer resistance R_{CT} , and the double layer capacitance, C_{dl} . C_{dl} was calculated from Nyquist plot using equation (4).

$$C_{dl} = \frac{1}{2\pi f_m R_{CT}}, \tag{4}$$

where C_{dl} = double layer capacitance, R_{CT} = charge transfer resistance, and f_m is the frequency at which the maximum imaginary impedance was observed.

Figure 11 reveals the Bode plots for rGO-b, rGO-m and rGO-p, as obtained from the electrochemical impedance spectroscopy. The capacitance can be written as a sum of real and imaginary capacitances as in equation (5).

$$C(f) = C'(f) + C''(f) \tag{5}$$

The real capacitance C' signifies the actual amount of charge delivered from the stored charges in the supercapacitor. Whereas, the imaginary capacitance C'' associates with the dissipative capacitive-energy through various

Table 3. Specific capacitance and characteristic resistances obtained from electrochemical impedance spectroscopy.

Sample name	R_s (Ω)	R_{CT} (Ω)	C_{dl} (μF cm ⁻²)
rGO-b	8.7	43.3	46.3
rGO-m	4.8	84.8	33.5
rGO-p	6.2	48.6	36.4

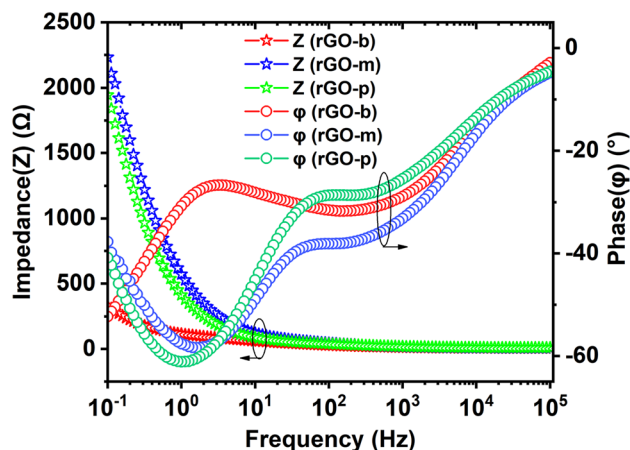


Figure 11. Bode plots for rGO-b, rGO-m and rGO-p.

irreversible losses such as dielectric loss, resistive loss etc. C' and C'' were estimated as functions of applied frequency with equations (6 and 7), respectively [23].

$$C'(f) = \frac{-Z''(f)}{2\pi f |Z(f)|^2} \tag{6}$$

$$C''(f) = \frac{Z'(f)}{2\pi |Z(f)|^2} \tag{7}$$

As evident from figure 12, the capacitance reaches high at low frequency below 1 Hz, where the phase also lags by approximately 65° leaning towards the capacitive nature. At high frequency on the other hand, the system behaves more like a resistive network with a significantly low capacitance and a near 0° phase-lag.

Comparing the FESEM results, it can be seen that the rGO-b has more significant gaps between the layers and has the highest surface roughness, which suggests a larger surface area with electrochemically active sites. That might be a reason behind the better electrochemical performance of rGO-b. Further, the UV-vis indicates a better reduction in rGO-b. Since deoxygenation restores the sp² carbons and enhances the electrical conductivity, this might be another factor supporting the enhanced SC value. Interestingly, in the Raman analysis, the rGO-b exhibited the I_D/I_G ratio higher than that of rGO-m, indicating fewer defects in the sp² carbon structure. It might be another fact behind increasing the I_D/I_G , such as the shrinkage of the average domain size of the sp² carbon structure and the increase in the number of domains [24]. So, although defect-free sp² carbons are forming, we observe a higher I_D/I_G due to the formation of smaller domains. One more possibility is the increase of the fractional graphene edges, which will also lead to increased I_D/I_G [4]. For every material, the SC is decreased with the increase of s.r. in CV or current density in GCD, which may be due to the limited time available for the effective charge transfer among the active material and the electrolyte solution.

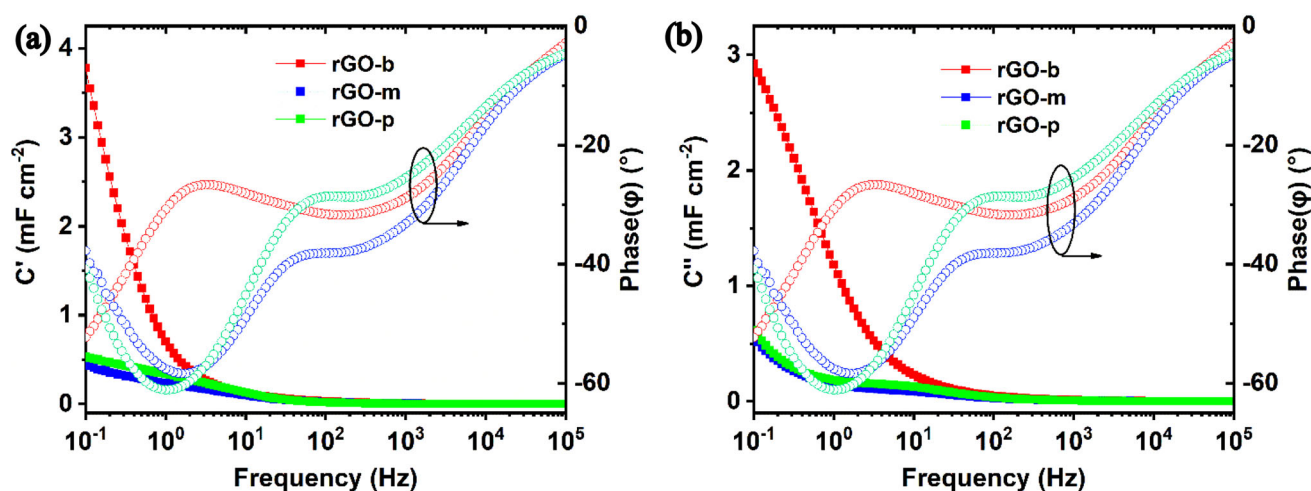


Figure 12. Frequency dependency of (a) real (C') and (b) imaginary capacitances (C'').

5. Conclusion

GO was successfully reduced using three green reductants banana, mango and potato extracts. XRD results of GO showed the peak at 11.01° , which attributes to the GO(001) plane, while rGO-b, rGO-m and rGO-p showed peaks in the range of 21° – 25° , which attribute to the rGO(002) plane. In the Raman analysis, appearance of the G peak indicated the existence of the sp^2 C=C structure. The FTIR of rGO showed an absorption peak at 1623.0 cm^{-1} , corresponding to the C=C bond, which is the backbone of the graphene structure. The CV results showed rGO-b with the highest SC of 176 F g^{-1} at 5 mV s^{-1} s.r. The GCD and EIS analyses also showed that the highest SC among the three samples was obtained from rGO-b. From the FESEM micrographs, it was found that rGO-b has higher surface roughness than rGO-m and rGO-p. The C/O ratio showed a slightly better reduction of rGO-b compared to that of rGO-m and rGO-p. This work explores and compares three different green reducing agents for reducing GO in an eco-friendly and inexpensive way, which can be helpful in energy storage applications.

Acknowledgements

We would like to thank Dr L Herojit Singh for facilitating UV–vis. We also acknowledge the School of Advanced Materials Engineering, Industry-Academic Cooperation Foundation, Kookmin University, Korea, for providing FESEM facilities.

References

- [1] Nongthombam S, Devi N A, Sinha S, Bhujel R, Rai S, Ishwarchand W *et al.* 2020 *J. Phys. Chem. Solids* **141** 109406
- [2] Lee K, Yoo Y K, Chae M S, Hwang K S, Lee J, Kim H *et al.* 2019 *Sci. Rep.* **9** 1
- [3] Bhujel R, Rai S, Deka U, Sarkar G, Biswas J and Swain B P 2021 *Bull. Mater. Sci.* **44** 2
- [4] Bo Z, Shuai X, Mao S, Yang H, Qian J, Chen J *et al.* 2014 *Sci. Rep.* **4** 4684
- [5] Sinha S, Devi N A, Nongthombam S, Bhujel R, Rai S, Sarkar G *et al.* 2020 *Diam. Relat. Mater.* **107** 107885
- [6] Guex L G, Sacchi B, Peuvot K F, Andersson R L, Pourrahimi A M, Ström V *et al.* 2017 *Nanoscale* **9** 27
- [7] Bhattacharya G, Sas S, Wadhwa S, Mathur A, McLaughlin J and Roy S S 2017 *RSC Adv.* **7** 26680
- [8] Moosa A A and Jaafar J N 2017 *J. Nanosci. Nanotechnol.* **7** 38
- [9] Zhang J, Yang H, Shen G, Cheng P, Zhang J and Guo S 2010 *Chem. Commun.* **46** 1112
- [10] Suresh D, Udayabhanu, Nagabhushana H and Sharma S C 2015 *Mater. Lett.* **142** 4
- [11] Kuila T, Bose S, Khanra P, Mishra A K, Kim N H and Lee J H 2012 *Carbon* **50** 914
- [12] Singh W I, Sinha S, Devi N A, Nongthombam S, Laha S and Swain B P 2020 *Polym. Bull.* **78** 6613
- [13] Sadhukhan S, Ghosh T K, Rana D, Roy I, Bhattacharyya A, Sarkar G *et al.* 2016 *Mater. Res. Bull.* **79** 41
- [14] Montelongo R G, Lobo M G and González M 2010 *Food Chem.* **119** 1030
- [15] Waghmare J S and Kurhade A H 2014 *Eur. J. Exp. Biol.* **4** 10
- [16] Nongthombam S, Sinha S, Devi N A, Laha S and Swain B P 2022 *Arab. J. Sci. Eng.* **47** 1–10
- [17] Singh W I, Sinha S, Devi N A, Nongthombam S, Laha S and Swain B P 2022 *Arab. J. Sci. Eng.* **47** 925
- [18] Sinha S, Singh W I, Nongthombam S, Devi N A, Laha S, Swain B S *et al.* 2022 *J. Phys. Chem. Solids* **161** 110478
- [19] Devi N A, Nongthombam S, Sinha S, Bhujel R, Rai S, Singh W I *et al.* 2020 *Diam. Relat. Mater.* **104** 107756
- [20] Liang H F, Smith C T G, Mills C A and Silva S R P 2015 *J. Mater. Chem. C* **3** 12484
- [21] Alfaraj N, Alghamdi W, Alawein M, Ajja I A, Priante D, Janjua B *et al.* 2020 *ACS Appl. Electron. Mater.* **2** 409

- [22] Devi N A, Sinha S, Nongthombam S and Swain B P 2022 *Mater. Sci. Semicond. Process.* **137** 106212
- [23] Sidhu N K and Rastogi A C 2016 *Synth. Met.* **219** 1
- [24] Stankovich S, Dikin D A, Piner R D, Kohlhaas K A, Kleinhammes A, Jia Y *et al.* 2007 *Carbon* **45** 1558